Theoretical and Experimental Investigations on the Novel Involute-Helix Gear Drive

Dong Liang[*], Bingkui Chen, Haixiang Li and Yane Gao

State Key Laboratory of Mechanical Transmission, Chongqing University, No. 174 Shazheng Street, 400030 Chongqing, China

Abstract: The theoretical and experimental investigations on involute-helix gear drive are carried out in this paper. Based on the generation principle and mathematical models, parametric design for tooth profiles is provided and three-dimensional solid models are established for simulation of motion. The general characteristics of involute-helix gears are discussed including undercutting condition, the separability of central distance, sliding and meshing characteristics. The meshing essence of tooth surfaces is revealed. Transmission efficiency experiment is made based on the developed gear prototype and the influence factors for the obtained results are also shown.

1. INTRODUCTION

Involute gearing has found widespread applications due to its simplicity for manufacture, mesh in line contact, constancy of meshing angle, and insensitivity to central distance variation [1]. The characteristics make them not only suitable for parallel axis transmission, but also to cases with intersecting or skew axes. However, the involute profile has the problems of relatively low-contact load capacity, poor lubrication and proneness to interference, which cannot satisfy the current requirements for high performance [2].

Many studies have been carried out to develop various concepts, design and analysis approaches toward this destination and a series of novel gear drives are also proposed to improve the transmission performance and fulfill different requirements [3-11]. According to the aforementioned research, the novel involute-helix gear drive characterized by the advantages of involute and circular-arc gears has been put forward by the authors [12]. It has point contact with the convex and concave circular-arc tooth profiles and the contact tracing line of tooth surfaces is an involute-helix curve whose projection on the gear end-face is a segment of involute.

The generation principle and mathematical models were developed based on the proposed theory of conjugate curves [12-14]. To evaluate the gear performance and reveal the good transmission characteristics, the further theoretical and experimental investigations on this gearing will be carried out, which is also of importance from the engineering application perspective. The remainder of this article is organized into four sections. In the following section, the geometric design of involute-helix gear drive is introduced. According to the given involute-helix curve, the general characteristics of this transmission are developed in the next section. The subsequent section analyzes the transmission efficiency of gear prototype. Finally, a conclusive summary of this study is given in the last section.

2. GEOMETRIC DESIGN OF INVOLUTE-HELIX GEAR PAIR

2.1. Generation Method and Mathematical Models

The tooth surfaces of involute-helix gears are generated based on the theory of conjugate curves. There are four steps for the generation processes [13-14]:

(1)   Solution of the conjugated curve in the given contact position according to the given involute-helix curve.

(2)   Equidistant motion along the designated normal vector for the conjugate-curve pair. Specially, the radius of concave tooth profile is slightly larger than that of convex tooth profile. The equidistance in a convex tooth is along the positive direction of common normal while it is reverse in a concave tooth.

(3)   Generation of the spherical enveloping surface of the equidistant curve based on the envelope theory of single parameter family.

*Address correspondence to this author at The State Key Laboratory of Mechanical Transmission, Chongqing University, No. 174 Shazheng Street, 400030 Chongqing, China; Tel: +86-23-65106247; Fax: +86-23-65106247; E-mail: liangdong_cqu@163.com
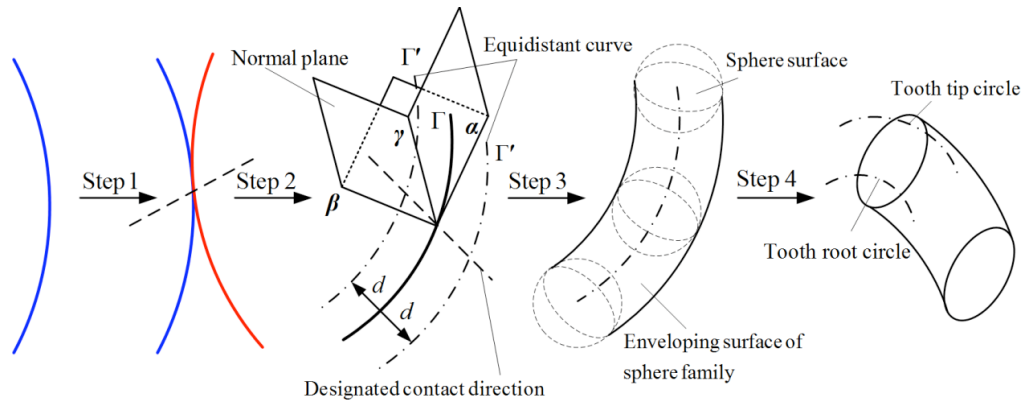
Figure 1: Generation processes of tooth surfaces.

(4)   Determination of tooth profiles inheriting the meshing characteristics of conjugate involute-helix curves in the limited range with the addendum and addendum cylinder surfaces.

Based on the simplified generation processes shown in Figure **1**, the mathematical models are established and the equations of tooth surfaces of the driving pinion and driven gear are derived as

$$\begin{cases} x_{\Sigma 1} = x_{hx1} + h_1 \cos\varphi \cos\alpha' \\ y_{\Sigma 1} = y_{hy1} + h_1 \cos\varphi \sin\alpha' \\ z_{\Sigma 1} = z_{hz1} + h_1 \sin\varphi \\ x'_{hx1}(\theta)\cos\alpha' + y'_{hy1}(\theta)\sin\alpha' + z'_{hz1}(\theta)\tan\varphi = 0 \end{cases} \quad (1)$$

and

$$\begin{cases} x_{\Sigma 2} = x_{hx2} + h_2 \cos\varphi \cos\alpha' \\ y_{\Sigma 2} = y_{hy2} + h_2 \cos\varphi \sin\alpha' \\ z_{\Sigma 2} = z_{hz2} + h_2 \sin\varphi \\ x'_{hx2}(\theta)\cos\alpha' + y'_{hy2}(\theta)\sin\alpha' + z'_{hz2}(\theta)\tan\varphi = 0 \end{cases} \quad (2)$$

where θ is the curve parameter. h_1, h_2 are the designated equidistance for different curves. x_{hx1}, y_{hy1}, z_{hz1} are the coordinate components of equidistant curve of the given involute-helix curve. x_{hx2}, y_{hy2}, z_{hz2} are the coordinate components of equidistant curve of the conjugated curve. φ, α' are the parameters of spherical enveloping surface. The variation range of the parameter φ is $-0.5\pi \le \varphi \le 0.5\pi$, whereas for α' the range is $0 \le \alpha' < 2\pi$.

2.2. Parametric Design of Tooth Profiles

According to aforementioned approach, the normal sections of convex and concave tooth profiles are developed, respectively. The mating tooth profiles are designed as displayed in Figure **2**. And it mainly contains three parts: the contact region, tooth fillet and tip/root limit. The parametric items of tooth profiles are given in Table **1**.

The convex and concave tooth profiles mesh in point contact. The ideal contact condition can be realized considering the conjugate-curve pair and optional contact direction simultaneously. As depicted
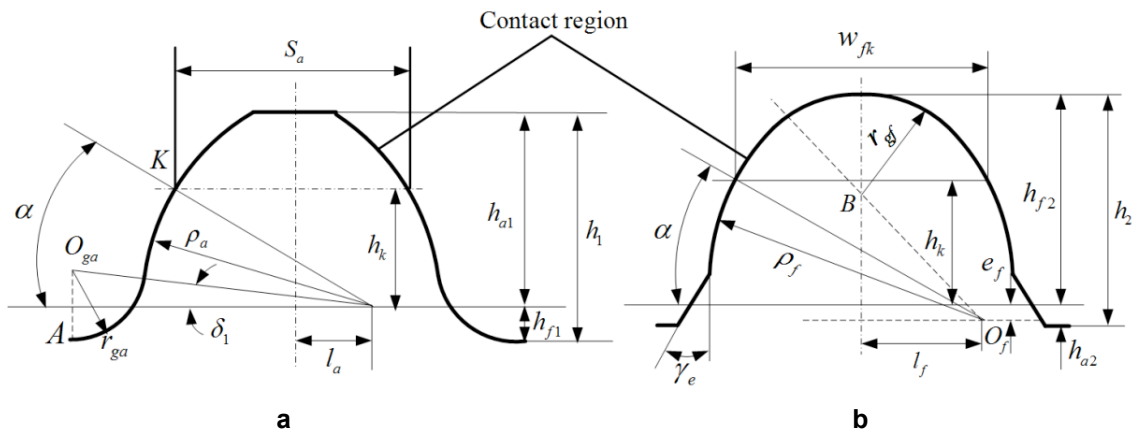

Figure 2: Tooth profiles in normal section: (**a**) convex tooth profile; (**b**) concave tooth profile.

Table 1:   Parametric Design of Tooth Profiles of Involute-Helix Gears

Parameters	Convex tooth profile	Concave tooth profile
Pressure angle α	20°~35°	20°~35°
Tooth height $h_i(i=1, 2)$	$1.5m_n$	$1.52m_n$
Tooth addendum height $h_{ai}(i=1, 2)$	$1.2339m_n$	$0.1661m_n$
Tooth dedendum height $h_{fi}(i=1, 2)$	$0.2661m_n$	$1.3539m_n$
Radius of circular-arc tooth profile $\rho_i(i=a, f)$	$1.5m_n$	$1.52m_n$
Movement distance of circle centre $e_i(i=a, f)$	0	$0.01m_n$
Offset distance of circle centre $l_i(i=a, f)$	$0.5895m_n$	$0.5596m_n$
Distance between contact point and pitch curve h_k	$0.6339m_n$	$0.6339m_n$
Tooth thick in contact point $S_i(i=a, f)$	$1.54m_n$	$1.54m_n$
Tooth space in contact point $\omega_{ik}(i=a, f)$	$1.6016m_n$	$1.5416m_n$
Tooth crack j	0	$0.05m_n$
Circle radius of tooth root $r_{gi}(i=a, f)$	$0.4m_n$	$0.452m_n$
Process angle $\delta_i(i=a, f)$	4°2′31″	4°52′55″
Addendum chamfer angle of concave tooth γ_e	none	45°

$*m_n$ represents the normal modulus.

in Figure **3**, the tooth profiles contact in unique point which is also the common tangent point. Γ_1 and Γ_2 are the conjugate involute-helix curves. Σ_1 and Σ_2 are the generated tooth surfaces.
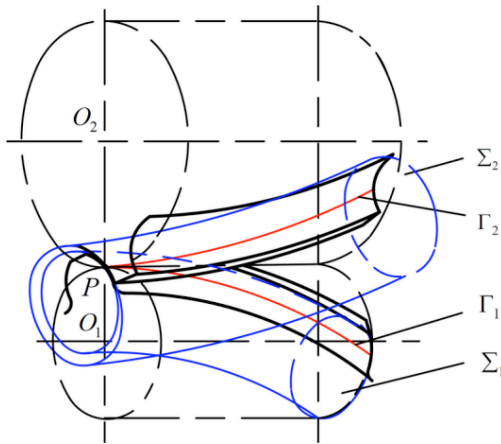

Figure 3: Point contact of mating tooth profiles.

2.3. Three-Dimensional Solid Models

The meshing surfaces of convex and concave tooth profiles are established based on the previous study. According to the developed equations in Ref. [12], a computer program for mathematical calculation based on MATLAB software is developed. The results are integrated and exported to the 3D drawing software UG and the precise three-dimensional solid models of gears can be created based on the geometric parameters in Table **2**.

Based on the established models in Figure **4**, a computerized simulation of meshing process is carried out in order to demonstrate its feasibility and evaluate the contact conditions. The results are observed as follows: (1) the gears can transmit rotational motion with a constant gear ratio and continuous transmission between two mating tooth surfaces; (2) tooth surfaces

Table 2:   Geometric Parameters of Involute-Helix Gear Drive

Parameters	Values	Parameters	Values
Radius of pitch circle of pinion r_1	22mm	Radius of tooth profile of pinion ρ_1	4mm
Radius of pitch circle of gear r_2	68mm	Radius of tooth profile of gear ρ_2	4.4mm
Module m_n	4mm	Helix parameter p	28.6478
Tooth number of pinion Z_1	11	Equidistant distance of pinion d_1	4mm
Tooth number of gear Z_2	34	Equidistant distance of gear d_2	4.4mm
Pressure angle α	30°	Tooth width B	30mm
Transmission ratio i_{21}	3.09	Range of curve parameter t	0~1.05rad

are in mesh with point contact along the conjugate curves in the axial direction, and the properties of curves are inherited with the process of meshing motion; (3) no meshing interference between the couple tooth surfaces can be found.
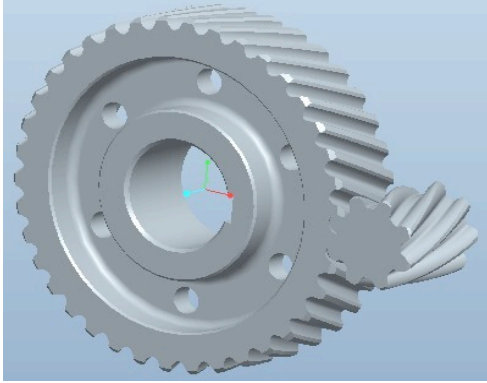

Figure 4: Three-dimensional solid models of involute-helix gears.

3. GENERAL CHARACTERISTICS OF GEAR DRIVE

3.1. Undercutting Condition

Tooth undercutting occurs when a singular point appears on the tooth surface. For the involute-helix gears, the pinion is more sensitive to undercutting due to the designed few numbers of teeth. Taking the single tooth flank as an example, the equation of contact region is expressed as

$$\begin{cases} x = \rho \sin\alpha - e \\ y = -(\rho \cos\alpha - l)\cos\beta + u\sin\beta \\ z = (\rho \cos\alpha - l)\sin\beta + u\cos\beta \end{cases} \quad (3)$$

Where ρ is the radius of convex tooth profile, e is movement distance of circle centre and l is offset distance of circle centre. α represents the pressure angle and β is helix angle. u expresses the displacement of tooth profile in axial direction.

The approach proposed by F.L. Litvin [15] is used to analyze this problem. Surface Σ_1 which is the tool surface represented in two-parameter form generates gear tooth surface Σ_2. Appearance of singular points on Σ_2 is the warning that the surface may be undercut in the process of generation. The definition of singularity of Σ_2 may be represented by equation $\mathbf{v}_r^{(2)} = 0$ and it has $\mathbf{v}_r^{(1)} + \mathbf{v}^{(12)} = 0$. Where the symbols $\mathbf{v}_r^{(2)}$ and $\mathbf{v}_r^{(1)}$ represent the relative velocity of contact point over tooth surfaces Σ_1 and Σ_2, respectively. $\mathbf{v}^{(12)}$ is the sliding velocity. Based on the previous study, this relationship can be obtained as $d[\Phi(t,\varphi,\alpha)] / ds = 0$,

where s is the introduced arc parameter. t is the curve parameter and φ,α are tooth surface parameters. According to the Ref. [14], $\Phi(t,\varphi,\alpha)$ represents the enveloping conditions of tubular tooth surfaces and it has $\Phi(t,\varphi,\alpha) \equiv (\mathbf{r}_t, \mathbf{r}_\varphi, \mathbf{r}_\alpha) = 0$. It allows us to determine a line on surface Σ_1 that generates singular points on Σ_2. According to gear geometry, it can be derived as

$$\begin{cases} \dfrac{\partial \mathbf{r}_1}{\partial t}\dfrac{dt}{ds} + \dfrac{\partial \mathbf{r}_1}{\partial \varphi}\dfrac{d\varphi}{ds} = -\mathbf{v}_1^{(12)} \\ \dfrac{\partial \Phi}{\partial t}\dfrac{dt}{ds} + \dfrac{\partial \Phi}{\partial \varphi}\dfrac{d\varphi}{ds} = -\dfrac{\partial \Phi}{\partial \alpha}\dfrac{d\alpha}{ds} \end{cases} \quad (4)$$

Here, $\partial \mathbf{r}_1 / \partial t$, $\partial \mathbf{r}_1 / \partial \varphi$ and $\mathbf{v}_1^{(12)}$ are three- or two-dimensional vectors for spatial and planar gearing, respectively. These vectors are represented in coordinate system S_1 which is connected to driving pinion 1 based on the principle of conjugate curves [13]. And equation (4) expresses a system of linear equations in two unknowns: dt / ds and $d\varphi / ds$, while $d\alpha / ds$ is considered as given. This system has a certain solution for the unknowns if the matrix

$$A = \begin{bmatrix} \dfrac{\partial \mathbf{r}_1}{\partial t} & \dfrac{\partial \mathbf{r}_1}{\partial \varphi} & -\mathbf{v}_1^{(12)} \\ \dfrac{\partial \Phi}{\partial t} & \dfrac{\partial \Phi}{\partial \varphi} & -\dfrac{\partial \Phi}{\partial \alpha}\dfrac{d\alpha}{ds} \end{bmatrix} \quad (5)$$

has the rank *r*=2. This yields

$$\Delta_2 = \begin{bmatrix} \dfrac{\partial x_1}{\partial t} & \dfrac{\partial x_1}{\partial \varphi} & -v_{x1}^{(12)} \\ \dfrac{\partial z_1}{\partial t} & \dfrac{\partial z_1}{\partial \varphi} & -v_{z1}^{(12)} \\ \dfrac{\partial \Phi}{\partial t} & \dfrac{\partial \Phi}{\partial \varphi} & -\dfrac{\partial \Phi}{\partial \alpha}\dfrac{d\alpha}{ds} \end{bmatrix}, \quad \Delta_1 = \begin{bmatrix} \dfrac{\partial x_1}{\partial t} & \dfrac{\partial x_1}{\partial \varphi} & -v_{x1}^{(12)} \\ \dfrac{\partial y_1}{\partial t} & \dfrac{\partial y_1}{\partial \varphi} & -v_{y1}^{(12)} \\ \dfrac{\partial \Phi}{\partial t} & \dfrac{\partial \Phi}{\partial \varphi} & -\dfrac{\partial \Phi}{\partial \alpha}\dfrac{d\alpha}{ds} \end{bmatrix},$$

$$\Delta_3 = \begin{bmatrix} \dfrac{\partial y_1}{\partial t} & \dfrac{\partial y_1}{\partial \varphi} & -v_{y1}^{(12)} \\ \dfrac{\partial z_1}{\partial t} & \dfrac{\partial z_1}{\partial \varphi} & -v_{z1}^{(12)} \\ \dfrac{\partial \Phi}{\partial t} & \dfrac{\partial \Phi}{\partial \varphi} & -\dfrac{\partial \Phi}{\partial \alpha}\dfrac{d\alpha}{ds} \end{bmatrix}$$

Where $v_{x1}^{(12)}$, $v_{y1}^{(12)}$ and $v_{z1}^{(12)}$ are the coordinate components of velocity vector $\mathbf{v}_1^{(12)}$ in coordinate system S_1. Only the expressions of Δ_1, Δ_2 and Δ_3 should be applied for determination of singularity conditions for the generated tooth surface Σ_2.

Furthermore, a sufficient condition for singularity of Σ_2 can be represented by $\Delta_1^2 + \Delta_2^2 + \Delta_3^2 = F(t,\varphi,\alpha) = 0$.

Substituting Eq. (3) into the above equations, the undercutting condition of tooth surfaces is obtained as

$$\Delta_1 = -\rho\cos\alpha\sin\beta\frac{\partial\Phi}{\partial\alpha} - (-r_1\varphi_1 + y)\rho\sin\alpha\cos\beta\frac{\partial\Phi}{\partial\varphi} +$$
$$(-r_1\varphi_1 + y)\frac{\partial\Phi}{\partial t}\sin\beta + (z-x)\rho\sin\alpha\frac{\partial\Phi}{\partial\varphi} = 0 \tag{6}$$

$$\Delta_2 = (-r_1\varphi_1 + y)\rho\sin\alpha\sin\beta\frac{\partial\Phi}{\partial\varphi} - \rho\cos\alpha\cos\beta\frac{\partial\Phi}{\partial\alpha} +$$
$$(-r_1\varphi_1 + y)\cos\beta\frac{\partial\Phi}{\partial t} + (-r_1\varphi_1 + y)\rho\cos\alpha\frac{\partial\Phi}{\partial\varphi} = 0 \tag{7}$$

$$\Delta_3 = (z-x)\rho\sin\alpha\sin\beta\frac{\partial\Phi}{\partial\varphi} + \rho\sin\alpha\cos\beta\frac{\partial\Phi}{\partial\alpha} + (-r_1\varphi_1 + y)$$
$$\sin\beta\frac{\partial\Phi}{\partial t} + (z-x)\cos\beta\frac{\partial\Phi}{\partial t} + (-r_1\varphi_1 + y)\rho\sin\alpha\cos\beta\frac{\partial\Phi}{\partial\varphi} = 0 \tag{8}$$

Where

$$\varphi_1 = \frac{1}{r_1}[\frac{\cos\alpha\cos\beta(x+z)}{\sin\alpha + \cos\alpha\sin\beta} + y];$$

$$\frac{\partial\Phi}{\partial\alpha} = -r_1(\sin\alpha + \cos\alpha\sin\beta);$$

$$\frac{\partial\Phi}{\partial\varphi} = \sin\alpha\sin\beta + \cos\alpha;$$

$$\frac{\partial\Phi}{\partial t} = \rho\sin\alpha\cos\beta(\sin\alpha + \cos\alpha\sin\beta) + (x+z)\sin\alpha\cos\beta$$
$$+ (\cos\alpha - \sin\alpha\sin\beta)(-r_1\varphi_1 + y + \rho\cos\alpha\cos\beta)$$

There is a simple way to avoid singularity and undercutting of a generated surface, it has

$$\begin{cases} \boldsymbol{r_1} = \boldsymbol{r_1}(t,\varphi) \\ \Phi(t,\varphi,\alpha) = 0 \\ F(t,\varphi,\alpha) = 0 \end{cases} \tag{9}$$

The equations determine a line which has to limit the generating surface Σ_1. In many cases, this can be achieved by choosing appropriate settings for surface Σ_1 that generates Σ_2.

3.2. The Separability of Central Distance

The influences on contact and bending stress of gear tooth are unavoidable due to center distance error. Because of the characteristics of involute tooth profile, this new gear transmission has the typical separability of center distance. The gear drive can keep the transmission ratio unchanged even if the central distance has changed. So the properties of the involute-helix gear are beneficial for its manufacturing, assembly and application.

The acute angle between the direction of circumferential velocity at the node P and line of action is called the meshing angle. The node P is the intersection between the common normal at the contact point of mating tooth profiles and the line connecting two circle centres of pinion and gear. According to the installation with standard center distance, the pitch circles of two gears and their reference circles coincide with each other, and the meshing angle is equal to the pressure angle of the reference circle. When the actual center distance a' and standard center distance a are
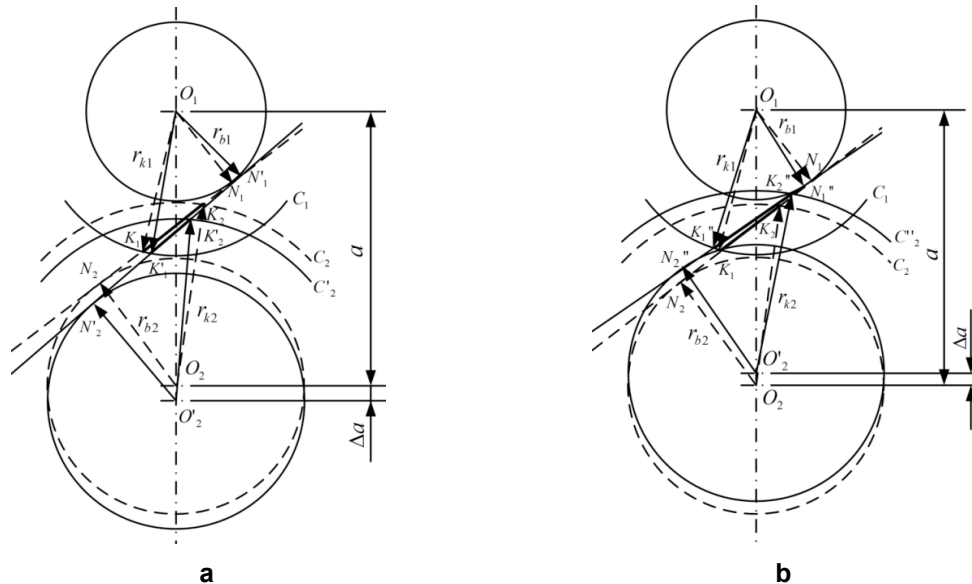

Figure 5: The changes of center distance: (**a**) increased center distance; (**b**) reduced center distance.

not the same, the reference circles cannot tangent with each other. The radius of the pitch circle is larger than that of the reference circle, then the corresponding meshing angle changes to $a'\cos\alpha' = a\cos\alpha$.

Figure **5a** reflects the change of actual meshing section on line of action under the case of increased center distance. In the case of standard center distance, the centers of convex and concave tooth gears locate on the points O_1 and O_2, respectively. The theoretical meshing segment is N_1N_2, and the actual track is K_1K_2. The entire contact traces within this range are involved in the mesh. We assume that the convex pinion is fixed and the center O_2 of concave gear moves down to O_2' along the center line of two gears. The error occurs while the center distance has been increased. It can be seen that the meshing angle, line of action and the node position also change. The theoretic mating segment is now $N_1'N_2'$, and the actual track has changed into $K_1'K_2'$. Only part of contact tracing line is in mesh but the transmission ratio still remains unchanged.

Figure **5b** depicts the change of actual meshing section on line of action under the case of reduced center distance. Through the analysis, the entire contact tracing lines are still involved in the mesh and the transmission ratio is also unvaried.

3.3. Sliding Characteristic

The general calculation method of sliding ratios of involute-helix gear pair is studied. Supposing a driving gear with original curve Γ_1 transmits movement to a driven gear with its conjugated curve Γ_2, they contact at point K as displayed in Figure **6**. ΔS_1 and ΔS_2 denote respectively the travelling arcs of conjugate curves Γ_1 and Γ_2 in a period of time Δt which approaches to zero during the meshing process. Assuming the relative
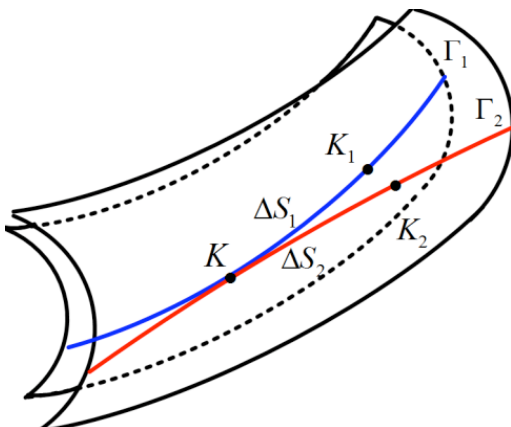

Figure 6: Sliding condition of tooth profiles.

sliding exists, the length of arc KK_1 is not equal to that of arc KK_2, and the difference between ΔS_1 and ΔS_2 is called the sliding arc. The sliding coefficient is analyzed as a ratio of the length of sliding arc relative to the length of the corresponding arc in meshing area.

The calculation formulas of sliding ratios of gear pair can be expressed as

$$\eta_1 = \lim_{\Delta S_1 \to 0} \frac{\Delta S_1 - \Delta S_2}{\Delta S_1} = \frac{\dfrac{dS_1}{dt} - \dfrac{dS_2}{dt}}{\dfrac{dS_1}{dt}} = \frac{dS_1 - dS_2}{dS_1} \tag{10}$$

and

$$\eta_2 = \lim_{\Delta S_2 \to 0} \frac{\Delta S_2 - \Delta S_1}{\Delta S_2} = \frac{\dfrac{dS_2}{dt} - \dfrac{dS_1}{dt}}{\dfrac{dS_2}{dt}} = \frac{dS_2 - dS_1}{dS_2} \tag{11}$$

Where

$$dS_1 = \sqrt{dx_1^2 + dy_1^2 + dz_1^2}\, dt$$
$$dS_2 = \sqrt{dx_2^2 + dy_2^2 + dz_2^2}\, dt$$

The parametric forms of conjugate involute-helix curves Γ_1 and Γ_2 are respectively expressed in Ref. [12]. The equation of given contact locus of pinion 1 is represented as

$$\begin{cases} x_1 = r\cos[(k+1)\theta + b] + r\theta\sin[(k+1)\theta + b] \\ y_1 = r\sin[(k+1)\theta + b] - r\theta\cos[(k+1)\theta + b] \\ z_1 = p(k\theta + b) \end{cases} \tag{12}$$

where r is the radius of basic circle. p is the screw parameter. θ is the involute parameter and the range of the variable is $\theta_1 \le \theta \le \theta_2$. θ_1 and θ_2 are the beginning and end values of involute parameter θ, respectively. B is the tooth width. $k = B/p(\theta_2 - \theta_1), b = -\theta_1 B/p(\theta_2 - \theta_1)$

It contains only single parameter θ in equation (12), and the form is a space involute which is spiral in nature. Based on the given curve of driving pinion 1, considering the transformation relation $r_2 = M_{21}r_1$ and the equation of meshing simultaneously, the equation of the conjugated curve of driven gear 2 is expressed as

$$\begin{cases} x_2 = r\cos[(i_{21}+1)\phi_1 + (k+1)\theta + b] + r\theta\sin \\ \quad [(i_{21}+1)\phi_1 + (k+1)\theta + b] - a\cos(i_{21}\phi_1) \\ y_2 = r\sin[(i_{21}+1)\phi_1 + (k+1)\theta + b] - r\theta\cos \\ \quad [(i_{21}+1)\phi_1 + (k+1)\theta + b] - a\sin(i_{21}\phi_1) \\ z_2 = p(k\theta + b) \\ U\cos\phi_1 - V\sin\phi_1 = W \end{cases} \tag{13}$$

Where
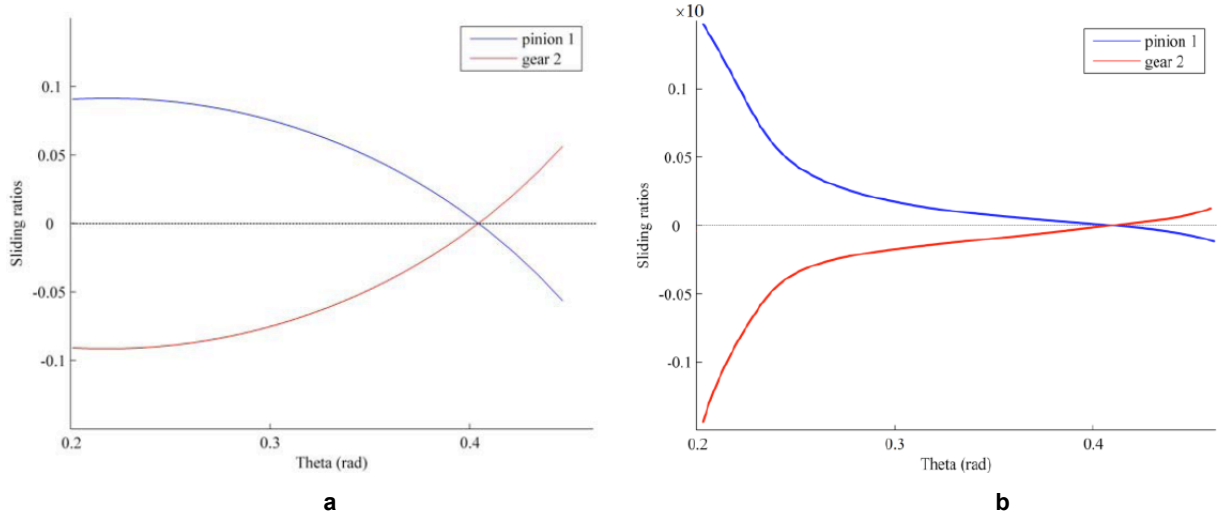
Figure 7: Sliding ratios of gears: **(a)** sliding ratios of involute-helix gears; **(b)** sliding ratios of involute gears.

$$U = -i_{21}a(un_{\beta y1} + vn_{\gamma y1});$$

$$V = i_{21}a(un_{\beta x1} + vn_{\gamma x1});$$

$$W = r(1+i_{21})\{\sin[(k+1)\theta + b] - \theta\cos[(k+1)\theta + b]\}$$

$$(un_{\beta x1} + vn_{\gamma x1}) - r(1+i_{21})\{\cos[(k+1)\theta + b] + \theta\sin$$

$$[(k+1)\theta + b]\}(un_{\beta y1} + vn_{\gamma y1})$$

i_{21} is the transmission ratio of gear pair. ϕ_1 and ϕ_2 are respectively the angular displacements of the driving gear 1 and driven gear 2. The relationship between ϕ_1 and ϕ_2 is $\phi_2 = i_{21}\phi_1$. $un_{\beta x1}$ and $un_{\beta y1}$ are the coordinate components of the principal normal vector under coordinate system S_1. $vn_{\gamma x1}$ and $vn_{\gamma y1}$ are the coordinate components of the binormal vector under coordinate system S_1.

Substituting the equations into equations (10) and (11), the sliding ratios of involute-helix gear drive can be obtained as

$$\eta_1 = 1 - \frac{\sqrt{\begin{array}{c}r^2 + r^2(\theta^2 + 1)[(i_{21}+1)\phi'_{1\theta} + (k+1)]^2 \\ +a^2 i_{21}^2 \phi'^2_{1\theta} + p^2 k^2\end{array}}}{\sqrt{r^2 k^2 + r^2\theta^2(k+1)^2 + p^2 k^2}} \qquad (14)$$

and

$$\eta_2 = 1 - \frac{\sqrt{r^2 k^2 + r^2\theta^2(k+1)^2 + p^2 k^2}}{\sqrt{\begin{array}{c}r^2 + r^2(\theta^2 + 1)[(i_{21}+1)\phi'_{1\theta} + (k+1)]^2 \\ +a^2 i_{21}^2 \phi'^2_{1\theta} + p^2 k^2\end{array}}} \qquad (15)$$

Where

$$\phi'_{1\theta} = \frac{1}{\sqrt{1 - \dfrac{W^2}{U^2 + V^2}}}\left(\frac{W}{\sqrt{U^2 + V^2}}\right)' + \frac{1}{1 + \left(\dfrac{U}{V}\right)^2}\left(\frac{U}{V}\right)'$$

Utilizing the mathematical parameters in Table **2**, the graph of sliding ratios between involute-helix gear pair is obtained. As shown in Figure **7a**, we can draw that: (1) the sliding coefficients during the engagement process are the function with respect to parameter θ; (2) the sliding coefficients of gear pair only pass through zero at the pitch point ($\theta = 0.403 rad$) and the symbols change due to the various direction of sliding velocity when the nearby contact points on both sides begin to mesh; (3) the maximum absolute values occur at the tooth root where the gear teeth mesh in and out. However, because of the contact of convex and concave tooth profiles, the absolute values of sliding coefficients are always smaller than 0.1 with the growth of parameter θ, which is close to 0. The sliding ratios of the corresponding in volute gear drive are also calculated and listed in Figure **7b** for comparison.

The comparison relationship of both gears is described. According to the developed results, the sliding coefficients of the involute-helix gear drive are smaller than that of involute gear drive, which can improve the transmission performance. The meshing can realize limit position and the approximate pure rolling contact may be accomplished. This method is suitable for arbitrary conjugate tooth profiles that contact along specific locus in axial direction, and it does not need to derive complicated geometrical relationship for calculation.

3.4. Meshing characteristic

The involute-helix gears mesh in point contact along the action line with the location change of the instantaneous contact point. A computer program is
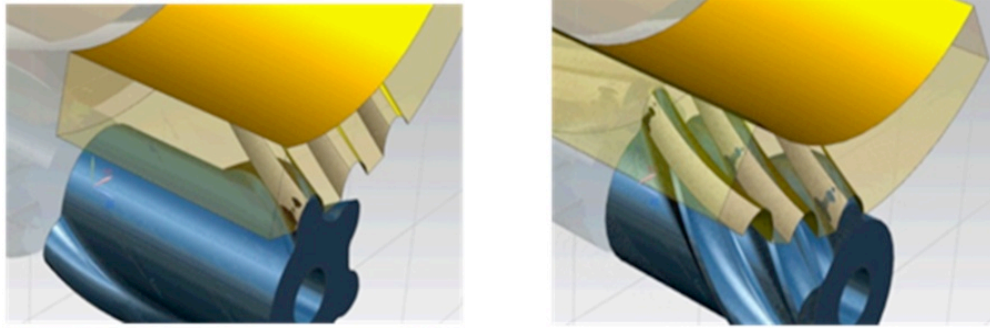
Figure 8: Meshing motion of tooth surfaces.

developed to simulate the meshing of tooth surfaces with UG software.

As shown in Figure **8**, the simplified model of convex and concave tooth surfaces is given. The engagement of tooth surfaces at the initial position is displayed in Figure **8(a)**. When the gear pair rotates with a fixed angular velocity, tooth profiles begin the continuous and tangent contact along conjugate involute-helix curves. The neighbouring points gradually follow into contact with the movement in the axial direction. The meshing condition at an arbitrary position is described in Figure **8(b)**. During the whole process, the convex and the concave tooth surfaces mesh in point contact. The instantaneous contact point of the conjugate curves moves along the line of action in the axial direction. The rolling diagram of the tooth surfaces of the gears is further shown in Figure **9**.
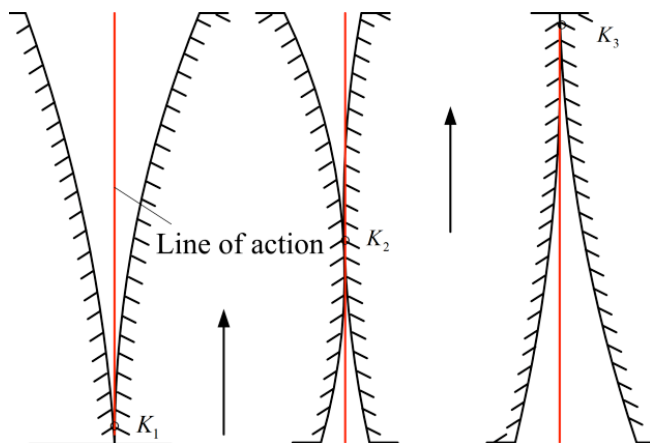
Figure 9: Rolling diagram of tooth surfaces.

It can be seen that the gears keep point contact with each other from initial position and separate at last. Line of action is depicted as a straight line. Throughout this process, contact point changes along the direction of line of action with those curves, and the line of action is a skew line whose projection on the gear end-face is the general meshing line of involute gearing.

Only a pair of conjugate curves maintains continuous and tangent contact with each other during motion, and the transmission process contains the meshing characteristics of conjugate curves. The engagement in the axial orientation between tubular tooth profiles has the same normal vector with conjugate curves at contact point. Through analysis, the normal for both meshing pair are coincident and the contact locus on mating tooth surfaces is also the conjugate involute-helix curve pair.

4. PERFORMANCE EXPERIMENT

For the two gears, they are processed with the hobbing cutters which fulfil the requirement of manufacturing precision. The hobs generated by rack cutters are designed and manufactured based on tubular tooth profiles. The hobbing trials have been carried out using YS3140CNC hobbing machine which is controlled by SIEMENS 840D system. It has the advantages of good transmission stability, working accuracy and operability. The hob cutting for generating the gears includes four movements: rotation of the workpiece about its axis, rotation of the hobbing cutter about its axis and feed motions of the hobbing cutter in radial and axial direction.

Figure 10: Gear prototype.

Table 3:   Performance Parameters of Equipments

| Equipment name	Model number	Performance parameters
1-Driving motor	YVPCG250M1-50	Power: 55 kWSpeed: 0-4500 rpm
2-Torque and rotational speed transducer I	JC1A	Nominal torque: 50 Nm
3- Gear Prototype	None	Centre distance: 90 mm Gear ratio: 3.09
4-Torque and rotational speed transducer II	NJ2A	Nominal torque: 2000 Nm
5- Gearbox reducer	CW100-63	Centre distance: 144 mm Gear ratio: 5
6-Loading motor	YVPCG315M3-16.7	Power: 55 kW Torque: 0-1051 Nm
7-Temperature transducer	WZP PT100	Temperature: -200°C-600°C

The pinion and gear based on the hob cutting principle are generated. The final accuracy of gear pair satisfies the design requirements according to the measurement of instrument. The final gear prototype is completed and depicted in Figure **10**.

The performance experiment of the reducer prototype had been made to evaluate its transmission property. For the investigation of operational characteristics, the layout of test system is considered. The equipments are linked by spring coupling. The input and output powers are measured with the each torque and rotational speed transducer. Oil temperature in the box is measured by the temperature transducer. Rotational speed is controlled by the variable speed electric motor, and the gear pair is loaded by the loading motor. The performance parameters of the equipments are listed in Table **3** and the trial site is shown in Figure **11**.

The contact point between the conjugate tooth profiles will spread over a small area under the load due to elastic deformations. So the contact condition is localized. Generally, the larger the contact area is, the higher the load capacities of gear drive will be. To achieve a better performance, it is necessary to carry

out the running-in process. It can expand the contact area for increasing the load capability and modify the gear tooth surfaces for reducing noise and vibration. The whole process was divided into five periods: Period one, after 2 hours' idle running with input shaft speed of 1250rpm, was followed by the second period of 2 hours with the operation under load (in this case the output torque is 300Nm). The third period lasted 2 hours under load (in this case the output torque is 400Nm). The fourth period lasted 2 hours under load (in this case the output torque is 500Nm) and the lasted period for another 2 hours under the load (in this case the output torque is 600Nm). After the 10 hours running-in period, the ideal contact condition is realized.

The input torque T_i and input shaft speed n_i can be measured by the torque and rotational speed transducer I, while the output values T_o and shaft speed n_o can be measured by the torque and rotational speed transducer II. The transmission efficiency can be calculated as $\eta = n_o T_o / n_i T_i$. The settings of test procedure are given as follows: the speeds are 500r/min, 750r/min, 1000r/min and 1250r/min, for the load, it is applied with 300Nm, 400Nm, 500Nm, and 600Nm. The
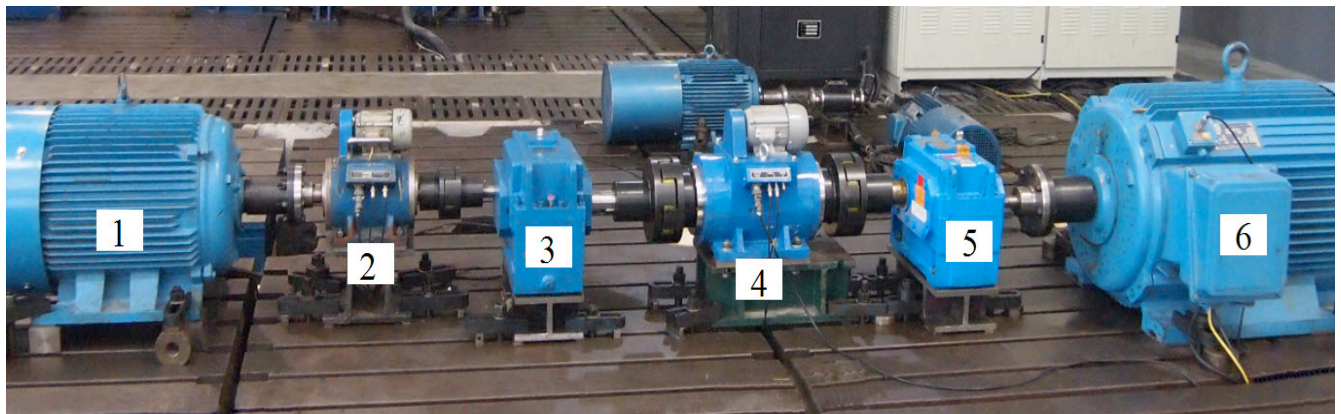
Figure 11: Testing site.

oil temperature which is corresponding to each stage is also recorded.

The transmission efficiency under different operating conditions is shown in Figure **12**. It can be concluded that the transmission efficiency will increase if increasing rotational speed and keeping torque constant. Similarly, it will also increase if increasing torque and keeping rotational speed constant. The maximum efficiency may be up to 96.9% at the load of 600Nm and the whole efficiency of prototype is in the range of 91.8%~96.9%. The oil temperature arrives at balance when the time is 60~70 Min. and its highest value is about 65.6°C with respect to the room temperature. Compared with conventional involute gear drive, the transmission efficiency of the proposed gear drive is probably lower. There are two main reasons affecting the transmission efficiency: (1) The mating gear pair is processed with the designed hobbing cutters. The tooth surfaces are only generated by the rough hob cutting process so that the manufacturing precision cannot fulfil the ideal requirement. (2) Because of the existence of machining errors and assembly errors in the involute-helix drive, the actual contact area may less than the theoretical contact area and the sliding between mating tooth surfaces also occurs.
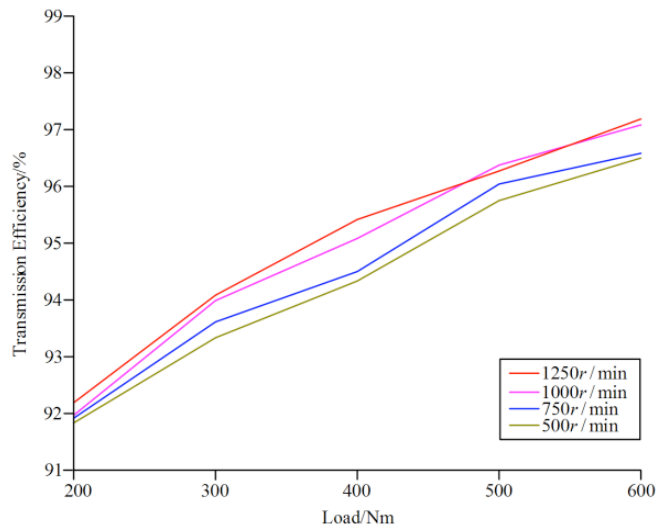

Figure 12: Transmission efficiency of proposed gears.

5. CONCLUSIONS

The parametric design of involute-helix gear drive is proposed based on the developed generation principle and mathematical model. The convex and concave tooth profiles are provided, respectively. According to the established solid models of gear pair, the

simulation of motion is carried out and the results show that it accords with the design expectation

The undercutting condition of mating tooth surfaces is provided. The separability of central distance of involute-helix gear drive is discussed. The results indicate that the transmission ratio remains unchanged even if the central distance has changed.

Based on the conjugate-curve pair, a calculation method for sliding ratios of this gearing is put forward and the result shows that the sliding coefficients are smaller than that of involute gear drive and the approximate pure rolling contact may be accomplished.

The point contact characteristic is studied. Only a pair of conjugate curves maintains continuous and tangent contact in the axial direction with each other. The normal for tooth surfaces and conjugate involute-helix curves at contact point are coincident and the contact locus on mating tooth surfaces is also the conjugate involute-helix curve pair.

The efficiency experiment of gear prototype is accomplished based on the manufactured pinion and gear designed by hobbing cutters. The maximum efficiency may be up to 96.9% at the load of 600Nm and the whole efficiency of prototype is in the range of 91.8%~96.9%. It shows the direct proportion with the change of rotational speed and torque.

ACKNOWLEDGEMENTS

REFERENCES

[1]   Luo SM, Wu Y, Wang J. The generation principle and mathematical models of a novel cosine gear drive, Mechanism and Machine Theory 2008; 43(12): 1543-1556.
http://dx.doi.org/10.1016/j.mechmachtheory.2007.12.007

[2]   Zhang H, Hua L, Han XH. Computerized design and simulation of meshing of modified double circular-arc helical gears by tooth end relief with helix, Mechanism and Machine Theory 2010; 45(1): 46-64.
http://dx.doi.org/10.1016/j.mechmachtheory.2009.08.001

[3]   Jywe WY, Hsu TH, Liu CH. Non-bar, an optical calibration system for five-axis CNC machine tools, International Journal of Machine Tools and Manufacture 2012; 59(8): 16-23.
http://dx.doi.org/10.1016/j.ijmachtools.2012.01.004

[4]   Bahk CJ, Parker RG. Analytical investigation of tooth profile modification effects on planetary gear dynamics, Mechanism and Machine Theory 2013: 70(12); 298-319.
http://dx.doi.org/10.1016/j.mechmachtheory.2013.07.018

[5]   Park D, Kahraman A. A surface wear model for hypoid gear pairs, Wear 2009: 267(9-10); 1595-1604.
http://dx.doi.org/10.1016/j.wear.2009.06.017

[6]   Wang J, Hou L, Luo SM, Wu RY. Active design of tooth profiles using parabolic curve as the line of action, Mechanism and Machine Theory 2013: 67; 47-63.
http://dx.doi.org/10.1016/j.mechmachtheory.2013.04.002

[7]   Litvin FL, Fuentes A, Zanzi C, Pontiggia M. Design generation and stress analysis of two versions of geometry of face gear drives. Mechanism and Machine Theory 2002: 37(10); 1179-1211.
http://dx.doi.org/10.1016/S0094-114X(02)00050-2

[8]   Chen CF, Tsay CB. Computerized tooth profile generation and analysis of characteristics of elliptical gears with circular arc teeth. Journal of Materials Processing Technology 2004; 148(2): 226-234.
http://dx.doi.org/10.1016/j.jmatprotec.2003.07.011

[9]   Li T, Pan CY, Gao FD, Wang XC. Research on sliding ratios of conjugate surfaces of two degrees of freedom meshing transmission of spherical gear pair, Journal of Mechanical design 2012; 134(9): 0910021-09100211.

[10] Tsai YC, Hsu WY. The study on the design of spiral bevel gear sets with circular-arc contact paths and tooth profiles, Mechanism and Machine Theory 2008: 43(9); 1158-1174.
http://dx.doi.org/10.1016/j.mechmachtheory.2007.08.004

[11] Chen CF, Tsay CB. Tooth profile design for the manufacture of helical gear sets with small numbers of teeth, International Journal of Machine Tools and Manufacture 2005; 45(12-13): 1531-1541.
http://dx.doi.org/10.1016/j.ijmachtools.2005.01.017

[12] Liang D, Chen BK, Gao YE. The generation principle and mathematical model of involute-helix gear transmission, Proceedings of the Institution of Mechanical Engineers, Part C. Journal of Mechanical Engineering Science 2013; 227(12): 2834-2843.
http://dx.doi.org/10.1177/0954406213478869http://dx.doi.org/10.1177/0954406213478869

[13] Chen BK, Liang D, Gao YE. The principle of conjugate curves for gear transmission, Journal of Mechanical Engineering 2014; 50(1): 130-136.
http://dx.doi.org/10.3901/JME.2014.01.130

[14] Chen BK, Gao YE, Liang D. Tooth profile generation of conjugate-curve gear, Journal of Mechanical Engineering 2014; 50(3): 18-24.
http://dx.doi.org/10.3901/JME.2014.03.018

[15] Litvin FL, Fuentes A. Gear Geometry and Applied Theory, second ed. Cambridge University Press, Cambridge 2004.
http://dx.doi.org/10.1017/CBO9780511547126